Quantum phase transition in spin-$\frac{1}{2}$ XX Heisenberg chain with three-spin interaction

Ping Lou,[1,2,*] Wen-Chin Wu,[1] and Ming-Che Chang[1]
[1]*Department of Physics, National Taiwan Normal University, Taipei 11650, Taiwan*
[2]*Department of Physics, Anhui University, Hefei 230039, Anhui, People's Republic of China*
(Received 18 August 2003; revised manuscript received 19 December 2003; published 5 August 2004)

The quantum phase transition in the spin-$\frac{1}{2}$ XX Heisenberg chain model with three-spin interaction is studied. Using the Jordan-Wigner transformation, several thermodynamic, as well as thermal and spin transport quantities of the system are calculated exactly. It is shown that the three-spin interaction influences the calculated quantities and leads to characteristic features of the quantum phase transition. The effects of a finite magnetic field on the magnetic moment and magnetic susceptibility are also discussed.

DOI: 10.1103/PhysRevB.70.064405 PACS number(s): 75.10.Jm, 75.40.Cx, 75.40.Gb, 71.27.+a

One of the most important ideas emerging from the studies of condensed matter physics in recent years is the concept of quantum criticality.[1] A quantum critical point marks a zero-temperature phase transition between different ground states of a many-body system as a result of change in parameters of the underlying Hamiltonian. Precisely at the quantum critical point, the system has no characteristic length or energy scale, and shows power-law spatial correlations and gapless excitations.

One-dimensional (1D) magnetic systems exhibit a variety of interesting phenomena signifying their quantum spin nature. Thus they have been the subject of intense theoretical and experimental studies. A great number of spin chain models have been proposed and investigated with various ranges of interaction, spin representations and anisotropies. The effects of the spin being coupled with other degrees of freedom have also been studied. Despite being unrealistic in some cases, the investigation of exactly solvable 1D quantum spin models can provide deep insight for understanding the characteristic phenomena occurring in real quasi-one-dimensional magnets. Moreover, the study of transport and response properties in exactly solvable 1D correlated fermion systems (e.g., the spinless fermion, the Hubbard, and other models) has long been an important field of theoretical research.

In this paper, we revisit the isotropic spin-$\frac{1}{2}$ XY (or spin-$\frac{1}{2}$ XX) chain model, which is related to the 1D antiferromagnet such as Cs_2CoCl_4.[2] Theoretically, the spin-$\frac{1}{2}$ XX chains provide an excellent ground for rigorous study of various properties of low-dimensional quantum magnetic systems.[3] By means of the Jordan-Wigner transformation, with which the spin model can be mapped onto a system of noninteracting spinless fermions, many thermodynamic calculations can be performed exactly. Because the model does not involve any competing interactions, there is no quantum critical point in this system, however. Here we shall explore an interesting spin-$\frac{1}{2}$ XX chain with three-spin interactions. This model not only exhibits a quantum critical point, but also is exactly solvable. Therefore the analysis of the effects of three-spin interactions on the thermodynamic, as well as thermal and spin transport properties can be studied in details.

The spin-$\frac{1}{2}$ XXZ chain with three-spin interaction was constructed by Tsvelik[4] and Frahm[5] using the quantum inverse scattering method. Their Hamiltonian can be expressed as

$$H=\sum_{l=1}^{N}-J(S_l^xS_{l+1}^x+S_l^yS_{l+1}^y+\Delta S_l^zS_{l+1}^z)-J'\{(S_{l-1}^xS_l^zS_{l+1}^y-S_{l-1}^yS_l^zS_{l+1}^x)+\Delta(S_{l-1}^yS_l^xS_{l+1}^z-S_{l-1}^zS_l^xS_{l+1}^y)+\Delta(S_{l-1}^zS_l^yS_{l+1}^x-S_{l-1}^xS_l^yS_{l+1}^z)\},\tag{1}$$

where S_l^α $(\alpha=x,y,z)$ are spin operators of $S=1/2$ spin on site l and N is the total number of spins, J is the nearest-neighbor Heisenberg exchange coupling, J' is the three-spin interaction strength, and Δ represents the anisotropy. This model exhibits several quantum phases depending on the parameters J'/J and Δ.[4,5] The same Hamiltonian is used in the study of current-carrying states for the system with *only* the nearest-neighbor interactions, where the three-spin terms play the role of the Lagrange multiplier.[6] In addition, the inclusion of four-spin interactions has also been investigated.[7] We shall apply the Jordan-Wigner (JW) transformation to the XXZ chain,

$$S_l^x=\frac{1}{2}\prod_{n=1}^{l-1}(1-2c_n^\dagger c_n)(c_l^\dagger+c_l);$$

$$S_l^y=\frac{1}{2i}\prod_{n=1}^{l-1}(c_l^\dagger-c_l)(1-2c_n^\dagger c_n);$$

$$S_l^z=c_l^\dagger c_l-\tfrac{1}{2}.\tag{2}$$

Notice that the Ising term in the XXZ model would lead to interacting JW fermions. But when $\Delta=0$, Hamiltonian (1) can be reduced to a free spinless fermion model, despite the presence of the three-spin term,

$$H=\sum_{l=1}^{N}\left[-\frac{J}{2}(c_l^\dagger c_{l+1}+\text{h.c.})+\frac{J'}{4i}(c_l^\dagger c_{l+2}-\text{h.c.})\right],\tag{3}$$

which can be diagonalized by means of the Fourier transformation. As a consequence,

$$H = \sum_k \varepsilon(k) c_k^\dagger c_k, \tag{4}$$

where the energy dispersion

$$\varepsilon(k) = -J\left[\cos k - \frac{\alpha}{2}\sin(2k)\right], \tag{5}$$

with $\alpha \equiv J'/J$.

It is apparent that the energy dispersion of the spinless fermion has the following features. When $\alpha \leqslant 1$, there are only two Fermi points at $\pm k_F = \pi/2$, the same feature as that of the isotropic XY model. But when α exceeds the critical value $\alpha_c = 1$, there are two negative-energy regions in k space, and four Fermi points appear. The two additional Fermi points appear at $k_F^1 = \arcsin(1/\alpha)$ and $k_F^2 = \pi - k_F^1$. In the thermodynamic limit, the ground state of the system corresponds to the configuration where all the states with $\varepsilon(k) \leqslant 0$ are filled and $\varepsilon(k) > 0$ are empty. Thus in the case of $\alpha < \alpha_c$, the ground state of the system corresponds to the configuration where all states with $|k| < k_F$ are filled. While for $\alpha > \alpha_c$, all the states with $-k_F < k < k_F^1$ and $k_F < k < k_F^2$ are filled. In this regard, it is naturally expected that there should occur a quantum phase transition when α gets across its critical value α_c. The new phase ($\alpha > \alpha_c$) is then characterized by two branches of incommensurate excitations, which are both gapless (see later). It is also important to note that because of the presence of three-spin interaction J' ($\alpha \neq 0$), $\varepsilon(k)$ is not symmetric under the change of $k \to -k$. This is in contrast to the isotropic XY model. Therefore, one expects naturally that in the presence of the three-spin interaction, some remarkable changes of the thermodynamic and transport properties of spin chains will occur.

We first investigate the ground state energy of the system,

$$E_0 = \sum_k \Theta[-\varepsilon(k)]\varepsilon(k). \tag{6}$$

Here the step function $\Theta(x) = 1$ when $x > 0$ and vanishes otherwise. A simple calculation gives

$$E_0(\alpha)/JN = \begin{cases} -\dfrac{1}{\pi} & \alpha \leqslant 1, \\ -\dfrac{1}{2\pi}\left(\dfrac{1}{\alpha} + \alpha\right) & \alpha > 1. \end{cases} \tag{7}$$

One can define a generalized stiffness, $\eta(\alpha) \equiv -\partial^2 E_0(\alpha)/\partial^2 \alpha$,[8] which is then given by

$$\eta(\alpha)/JN = \begin{cases} 0 & \alpha \leqslant 1, \\ \dfrac{1}{\pi}\dfrac{1}{\alpha^3} & \alpha > 1. \end{cases} \tag{8}$$

In Fig. 1, we plot the ground state energy $E_0(\alpha)$ and the generalized stiffness $\eta(\alpha)$ versus the parameter α. It is obvious that at $\alpha = \alpha_c$ the generalized stiffness is singular. This singularity marks the quantum phase transition in the ground state of the system as α is varied.[8]

We next calculate the magnetic moment for the ground states,

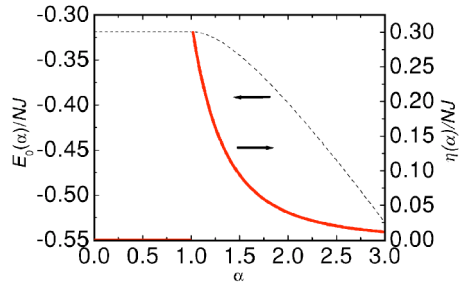

FIG. 1. The ground state energy $E_0(\alpha)/NJ$ and the generalized stiffness $\eta(\alpha)/NJ$ versus the parameter α.

$$M_z(\alpha) = \frac{1}{N}\sum_{l=1}^{N}\langle S_l^z\rangle = \frac{1}{2\pi}\int_{-\pi}^{\pi}\Theta[-\varepsilon(k)]dk - \frac{1}{2} = 0. \tag{9}$$

Hence for all values of α, the magnetization is zero. That is, the ground state of the new phase ($\alpha > 1$) exhibits no magnetic moment either. To characterize the ground state of the new phase, we study also the scalar chirality parameter, which is defined by[9,10]

$$O_\kappa = \frac{1}{N}\sum_{l=1}^{N}\langle \mathbf{S}_{l-1}\cdot\mathbf{S}_l \times \mathbf{S}_{l+1}\rangle. \tag{10}$$

It is obtained analytically that

$$O_\kappa(\alpha) = \begin{cases} 0 & \alpha \leqslant 1, \\ \dfrac{1}{2\pi}\left(1 - \dfrac{1}{\alpha^2}\right) & \alpha > 1. \end{cases} \tag{11}$$

Thus the ground state of the new phase is a chiral state ($O_\kappa > 0$) with gapless excitations. It is separated by the critical point $\alpha_c = 1$ from the ground state of normal ($O_\kappa = 0$) gapless phase.

In Fig. 2, we present the density of states (DOS) of spinless fermions,

$$\rho(\omega, \alpha) = \sum_k \delta[\omega - \varepsilon(k)], \tag{12}$$

for different values of the parameter α. When $\alpha = 0$, there are only two peaks (van Hove singularities) for $\rho(\omega, \alpha)$, occurring at the two band edges ($\omega = \pm J$). When $0 < \alpha < \alpha_c$, there appears a broad peak at the Fermi surface ($\omega = 0$). With the increase of α, the broad peak becomes sharper. It evolves into a very sharp peak at $\alpha = \alpha_c$ [see Fig. 2(c)], reflecting the flat-band behavior near $k = \pi/2$. While for $\alpha > \alpha_c$, the single sharp peak splits into two and locate at the two sides of the Fermi surface. These strong DOS peaks near or right at the Fermi surface (for $\alpha \geqslant \alpha_c$) are the main causes to the anomalous behaviors in various physical properties. In the following, we shall study the low-temperature behaviors of various thermodynamic and transport quantities exactly.

First, we consider the specific heat, which is given by ($k_B \equiv 1$)

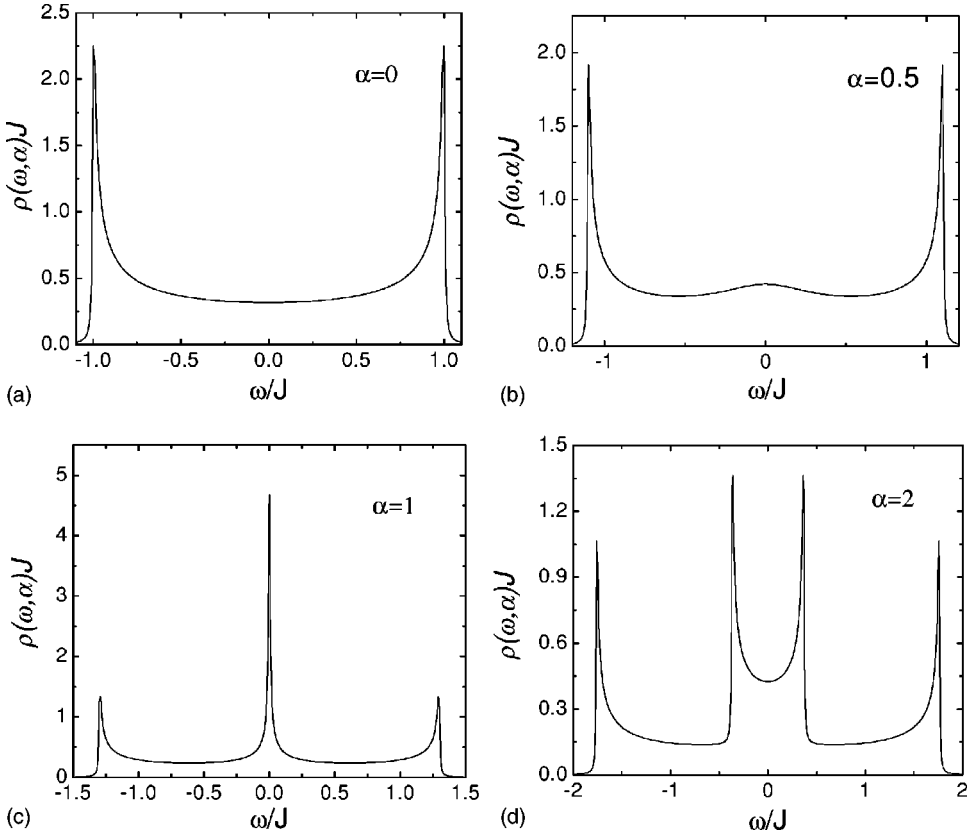

FIG. 2. The spinless fermion density of states $\rho(\omega,\alpha)J$ versus the scaled energy ω/J for different values of α.

$$C(T,\alpha)=\frac{\partial\langle H\rangle_T}{\partial T}=\frac{\partial}{\partial T}\left\{\sum_k \varepsilon(k)f[\varepsilon(k)]\right\}$$
$$=\sum_k\left\{\frac{\varepsilon(k)/2T}{\cosh[\varepsilon(k)/2T]}\right\}^2. \tag{13}$$

Here f is the Fermi distribution function. The specific heat of the system as a function of temperature T scaled to J is shown in Fig. 3 for different values of α. The anomalous temperature dependence in the vicinity of the quantum critical point is clearly seen. In contrast to the $\alpha=0$ case, the specific heat starts to gain more weight at the low temperatures when $\alpha\neq 0$. This is mainly caused by the broad peak of the spinless fermion DOS. Of most interest, a second peak structure in heat capacity appears at low temperature when $\alpha>\alpha_c$, a manifestation of the strong DOS peaks near the Fermi surface.

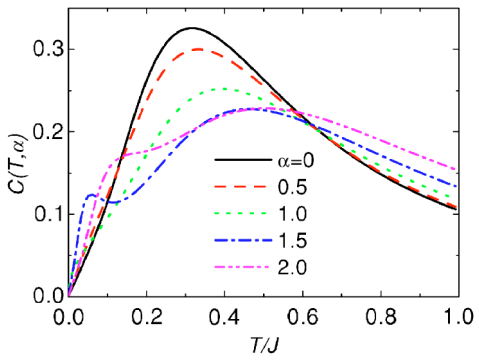

FIG. 3. The specific heat of the system $C(T,\alpha)$ versus the scaled temperature T/J for different values of α.

Another thermodynamic quantity is the magnetic susceptibility given by

$$\chi(T,\alpha)=\sum_k -\left\{\frac{\partial f[\varepsilon(k)]}{\partial\varepsilon(k)}\right\}=\frac{1}{4T}\sum_k\frac{1}{\cosh^2[\varepsilon(k)/2T]}. \tag{14}$$

At $T=0$, the magnetic susceptibility can be obtained analytically

$$\chi(\alpha)J=\begin{cases}\frac{1}{\pi}\frac{1}{1-\alpha^2} & \alpha<1,\\ \frac{1}{\pi}\frac{2\alpha}{\alpha^2-1} & \alpha>1,\end{cases} \tag{15}$$

which diverges at $\alpha=1$. In Fig. 4, the magnetic susceptibility of the system as a function of temperature is plotted for different values of α. The inset shows the α-dependence of χ at $T=0$. Once again, the singular $\chi(\alpha)$ at $T=0$ and $\alpha=\alpha_c$ marks the quantum criticality, which shows that the magnetic behavior of the system in the region $\alpha<1$ is different from that of the region $\alpha>1$.

The entropy of the system can also be obtained directly using the fermionic degrees of freedom. The calculated result is given below,

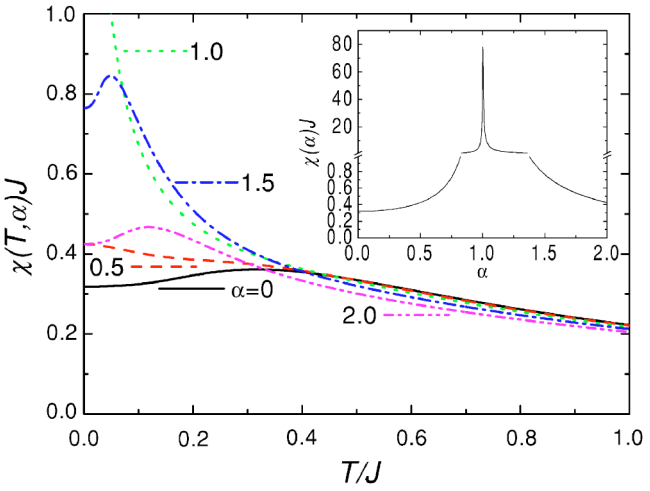

FIG. 4. The magnetic susceptibility of the system $\chi(T,\alpha)J$ versus the scaled temperature T/J for different values of α. The inset shows $\chi(\alpha)J$ versus α at $T=0$.

$$S = \sum_k \left\{ \ln[2\cosh[\varepsilon(k)/2T]] - \left(\frac{\varepsilon(k)}{2T}\right)\tanh[\varepsilon(k)/2T] \right\}. \tag{16}$$

The numerical result of $S(\alpha,T)$ versus the parameter α at $T=0.0001J$ is plotted in Fig. 5, in which a sharp peak at the critical value $\alpha_c=1$ can be observed.

Using a method adopted by Lieb, Schultz, and Mattis,[3] we can also calculate the spin-spin correlations exactly,

$$\begin{aligned}\rho_{l,l+m} &= \langle \mathbf{S}_l \cdot \mathbf{S}_{l+m} \rangle \\ &= \langle S_l^x S_{l+m}^x \rangle + \langle S_l^y S_{l+m}^y \rangle + \langle S_l^z S_{l+m}^z \rangle \\ &= \rho_{l,l+m}^x + \rho_{l,l+m}^y + \rho_{l,l+m}^z. \end{aligned} \tag{17}$$

It is obtained analytically that

$$\rho_{l,l+m}^x = \rho_{l,l+m}^y = \frac{1}{4}\begin{vmatrix} G_{l,l+1} & G_{l,l+2} & \cdots & G_{l,l+m} \\ G_{l,l} & G_{l,l+1} & \cdots & G_{l,l+m-1} \\ \cdots & \cdots & \cdots & \cdots \\ \cdots & \cdots & \cdots & \cdots \\ G_{l,l-m+2} & G_{l,l-m+3} & \cdots & G_{l,l+1} \end{vmatrix}, \tag{18}$$

and

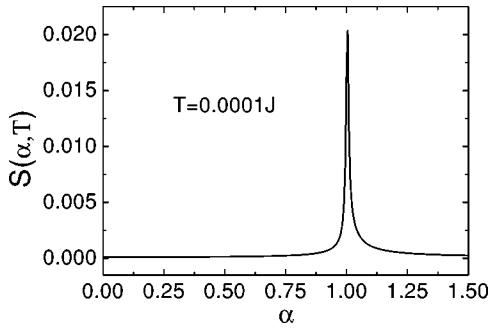

FIG. 5. The entropy $S(\alpha,T)$ of the system versus the parameter α at $T=0.0001J$.

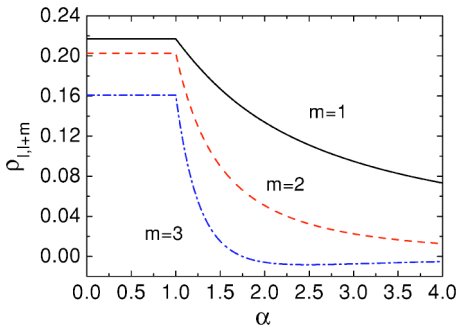

FIG. 6. The short-range orders $\rho_{l,l+m}(\alpha)$ of the system for $m=1$, 2, and 3 are plotted versus the parameter α at $T=0$.

$$\rho_{l,l+m}^z = -\tfrac{1}{4}(G_{l,l+m})^2, \tag{19}$$

with

$$G_{l,l+m} = \begin{cases} \dfrac{2}{m\pi}\sin\left(m\dfrac{\pi}{2}\right) & \alpha < 1, \\ \dfrac{1}{m\pi}[1-(-1)^m]\sin\left(m\arcsin\left(\dfrac{1}{\alpha}\right)\right) & \alpha \geqslant 1. \end{cases} \tag{20}$$

It is noted that because $\rho_{l,l+m}^z \leqslant 0$, it would decrease the total spin-spin correlations.

The short-range order is given

$$\rho_{l,l+1}(\alpha) = \begin{cases} \dfrac{\pi-1}{\pi^2} & \alpha < 1, \\ \dfrac{\pi\alpha-1}{(\pi\alpha)^2} & \alpha \geqslant 1. \end{cases} \tag{21}$$

For the correlation between the spins on sites separated by more than one lattice constant, we give the results for $m=2$ and 3. For $m=2$, we have

$$\rho_{l,l+2}(\alpha) = \begin{cases} \dfrac{1}{\pi^2} & \alpha < 1, \\ \dfrac{1}{(\pi\alpha)^2} & \alpha \geqslant 1. \end{cases} \tag{22}$$

While for $m=3$, we have

$$\rho_{l,l+3}(\alpha) = \begin{cases} \dfrac{48-\pi}{9\pi^3} & \alpha < 1, \\ \dfrac{48\alpha-\pi(3\alpha^2-4)^2}{(9\pi^3\alpha)^6} & \alpha \geqslant 1. \end{cases} \tag{23}$$

The numerical results for $\rho_{l,l+1}(\alpha)$, $\rho_{l,l+2}(\alpha)$, and $\rho_{l,l+3}(\alpha)$ versus the parameter α are plotted in Fig. 6. From the results above, we find the following characteristics of spin-spin correlations. First, there is no long-range order, as expected, because when $m\to\infty$, $\rho_{l,l+m}$ approaches zero. Second, the spin-spin correlations for the phase in $\alpha<1$ does not depend on the value of α, while for the new phase in $\alpha>1$, it decrease as α increases. Also, because the spin-spin correlations of the new phase is lower than that of the normal phase,

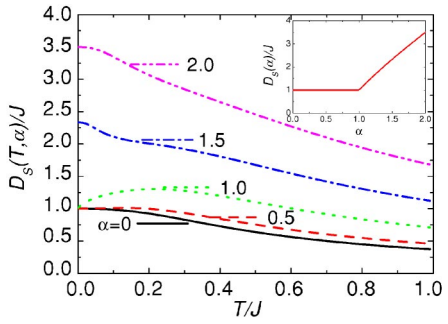

FIG. 7. Spin Drude weight $D_S(T,\alpha)/J$ versus the scaled temperature T/J for different values of α. The inset shows $D_S(\alpha)/J$ versus α at $T=0$.

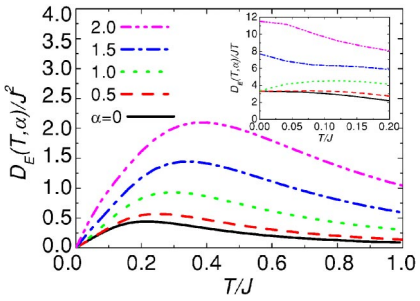

FIG. 8. Thermal Drude weight $D_E(T,\alpha)/J^2$ versus the scaled temperature T/J for different values of α. For easier comparison, the inset shows $D_E(\alpha)/JT$ versus T/J for different α's in the low-temperature regime.

the spin configuration in the new phase should be more disordered. We can see that the three-spin term causes quantum frustration, which eventually leads to the quantum phase transition in this system.

We now turn to the transport properties of the system. Very recently, thermal and spin transport in several integrable models of 1D spin systems have been studied employing the Kubo formalism and adopting the notion of the thermal and spin Drude weights,[11–13] which are similar to the Drude weight in the theory of electrical transport. Spin transport can be measured by NMR that probes the spin-spin autocorrelation in the low-frequency limit.[11] The spin Drude weight D_S (sometimes called the spin conductivity) is defined by[12]

$$D_S(T) = \frac{\pi}{ZNT} \sum_{\substack{m,n \\ E_m=E_n}} e^{-E_m/T} |\langle m|j_S|n\rangle|^2, \tag{24}$$

where Z is the partition function, $|n\rangle$ and E_n are the energy states and levels of the system, and the spin current operator is given as follows:

$$j_S = J\sum_{l=1}^{N} \left[\frac{1}{2i}(S_l^+ S_{l+1}^- - S_l^- S_{l+1}^+) - \alpha(S_l^+ S_{l+2}^- + S_l^- S_{l+2}^+) S_{l+1}^z \right]. \tag{25}$$

In the fermion representation, $j_S = \Sigma_k v(k) c_k^\dagger c_k$, where the velocity $v(k) = \partial\varepsilon(k)/\partial k = J[\sin k + \alpha\cos(2k)]$. Note that the periodic boundary condition has been applied. For the present spin system, D_S is simply reduced to

$$D_S(T,\alpha) = \frac{\pi}{4T}\sum_k \left\{ \frac{v(k)}{\cosh[\varepsilon(k)/2T]} \right\}^2. \tag{26}$$

At $T=0$, the spin conductivity is calculated to be

$$D_S(\alpha)/J = \begin{cases} 1 & \alpha \leqslant 1, \\ 2\alpha - \dfrac{1}{\alpha} & \alpha > 1. \end{cases} \tag{27}$$

In Fig. 7, we plot $D_S(T,\alpha)$ of the system as a function of temperature for different values of α. The inset shows the $D_S(\alpha)/J$ at $T=0$ versus the parameter α. Notice that at $T=0$, $D_S(\alpha)/J$ is *universal* for $\alpha \leqslant \alpha_c$, and it starts to grow up (as α increases) only for $\alpha > \alpha_c$. When $\alpha=0$, $D_S(T,\alpha)$ at very low T decrease quadratically with T.[14] Nonmonotonic behavior is observed for $\alpha=1$ and, as expected, the low-temperature behaviors of the spin conductivity are different for $\alpha < \alpha_c$ and $\alpha > \alpha_c$.

In a similar manner, the thermal conductivity D_E of the system is given by[12]

$$D_E(T) = \frac{\pi}{ZNT^2} \sum_{\substack{m,n \\ E_m=E_n}} e^{-E_m/T} |\langle m|j_E|n\rangle|^2 = \pi\sum_k \left\{ \frac{v(k)\varepsilon(k)/2T}{\cosh[\varepsilon(k)/2T]} \right\}^2, \tag{28}$$

where $j_E = \Sigma_k v(k)\varepsilon(k) c_k^\dagger c_k$ is the thermal current operator in the fermion representation, while in the spin representation it is given as

$$j_E = J^2\sum_{l=1}^{N} \left[-\frac{\alpha}{8}(S_l^+ S_{l+1}^- + S_l^- S_{l+1}^+) - \frac{i}{2}(S_l^+ S_{l+2}^- - S_l^- S_{l+2}^+) S_{l+1}^z - \frac{3\alpha}{2}(S_l^+ S_{l+3}^- + S_l^- S_{l+3}^+) S_{l+1}^z S_{l+2}^z + i\alpha^2 (S_l^+ S_{l+4}^- - S_l^- S_{l+4}^+) S_{l+1}^z S_{l+2}^z S_{l+3}^z \right]. \tag{29}$$

The behavior of $D_E(T)$ for different α's is shown in Fig. 8.[15] To show the characteristic difference more clearly between the cases of $\alpha < \alpha_c$ and $\alpha > \alpha_c$, we plot $D_E(T,\alpha)/T$ in the inset. Similar to the results of $D_S(T=0,\alpha)$ (see the inset of Fig. 7), as $T \to 0$, D_E/T is universal for $\alpha \leqslant \alpha_c$ and increases as α increases beyond $\alpha > \alpha_c$. One can obtain analytically that

$$\lim_{T\to 0} D_E(T,\alpha)/JT = \begin{cases} \dfrac{\pi^2}{3} & \alpha \leqslant 1, \\ \dfrac{\pi^2}{3}\left(2\alpha - \dfrac{1}{\alpha}\right) & \alpha > 1. \end{cases} \tag{30}$$

Finally, the effects of a finite magnetic field on the magnetic moment and the magnetic susceptibility are studied. When applying an external magnetic field h to the system,

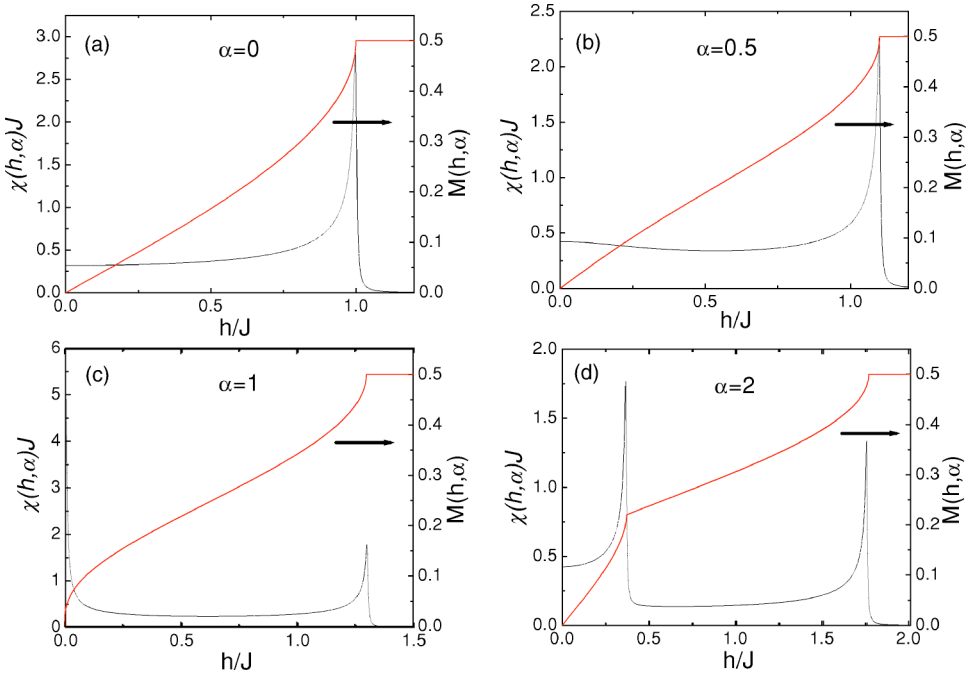

FIG. 9. The magnetic moment $M(h,\alpha)$ and magnetic susceptibility $\chi(h,\alpha)J$ of the system versus the uniform magnetic field h for different values of α at $T=0$.

the spinless fermion energy dispersion is changed to $\varepsilon(k) = -h - J[\cos(k) - (\alpha/2)\sin(2k)]$. At $T=0$, we have calculated the magnetic moment $M(h,\alpha)$ and magnetic susceptibility $\chi(h,\alpha)J$ of the system versus the uniform magnetic field h. The results are given in Fig. 9 for $\alpha=0$, 0.5, 1, and 2, respectively. It is shown in Fig. 9 that for $\alpha<1$, the magnetic moment and magnetic susceptibility curves shows no anomaly in the medium field region. In contrast, for $\alpha>\alpha_c$, the magnetic moment develops a cusp in the medium field region, and consequently a peak emerges in the magnetic susceptibility. In Fig. 10, we show how the position of the cusp in $M(h,\alpha)$ changes when varying $\alpha(\geqslant\alpha_c)$. It is noted that the position of the cusp moves to higher field as α increases, and the cusp disappears when $\alpha\to\infty(\alpha^{-1}=0)$. Similar cusp singularities have also been observed in the spin-1/2 zig–zag spin ladder, the spin-1 bilinear-biquadratic chain,[16]

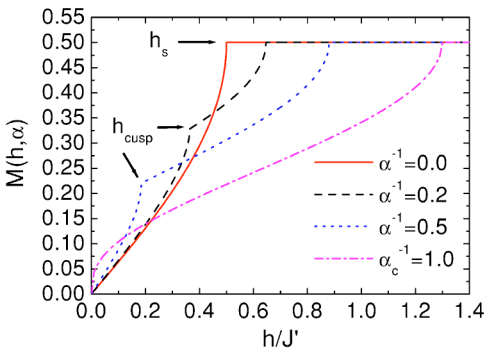

FIG. 10. The magnetic moment $M_z(h,\alpha)$ of the system versus the uniform magnetic field h (in units of J', instead of J) for $\alpha \geqslant \alpha_c$ at $T=0$. In the figure, h_s is the saturation field, and h_{cusp} is the field at the cusp.

and the frustrated Kondo necklace model.[17] The critical behaviors near the cusp singularity and the saturation singularity can be investigated using a method adopted by Yamamoto *et al.*[17] The result is

$$M - M_{\text{cusp}} \propto \begin{cases} h - h_{\text{cusp}} & h > h_{\text{cusp}} \\ -\sqrt{h_{\text{cusp}} - h} & h < h_{\text{cusp}}, \end{cases} \tag{31}$$

in the vicinity of the critical point $h=h_{\text{cusp}}$ where $M=M_{\text{cusp}}$. However, in the vicinity of the critical point $h=h_s$ (the saturation field), we have

$$M - M_s \propto \begin{cases} 0 & h \geqslant h_s \\ -\sqrt{h_s - h} & h < h_s. \end{cases} \tag{32}$$

When $\alpha\to\infty$, $h_{\text{cusp}}\to h_s$ and the cusp disappears. This explains nicely the behavior of the magnetization curves near the cusp singularity in the above calculations (see Figs. 9 and 10). The origin of the cusp in the present model is the same as that in the frustrated Kondo necklace model.[17] It is due to the change of the shape of the quasiparticle energy dispersion. For $h<h_{\text{cusp}}$, there are four Fermi points; while for $h>h_{\text{cusp}}$, there are only two Fermi points. This sudden change leads to a change of slope of the total energy at the critical point, and hence the cusp. Therefore, these cusps again reflect the competition between the two-spin J and three-spin J' interactions.

In summary, based on an exactly solvable model of the spin-$\frac{1}{2}$ XX Heisenberg chain with three-spin interactions, we have studied the thermodynamic and transport properties for the system. Quantum phase transition is realized in this exactly solvable model, which is caused by the competition between the two-spin J and three-spin J' interactions. The behaviors of density of states, magnetic susceptibility, spe-

cific heat, entropy, spin correlation, spin and thermal conductivities, and magnetic moment near the critical point ($J'/J=1$) are all studied exactly.

Note added in proof: After the paper was submitted, we were informed by the referee that Titvinidze and Japaridze[18] has published a similar work. Their Hamiltonian contains three-spin terms of the form $-J'\Sigma_l (S_l^x S_{l+1}^z S_{l+2}^x + S_l^y S_{l+1}^z S_{l+2}^y)$. There also exists two quantum phases in this model, which are separated by a critical value of $\alpha_c'=2$. Nevertheless, there are several crucial differences between these two models. First, their ground state has a spontaneous magnetization for almost all values of α, while ours always has zero magnetization. Second, the scalar chiral parameter for their model is zero, while ours can be nonzero when $\alpha>1$ [see Eq. (11)]. Third, the specific heat of their quantum phase with large α does not have the two-peak structure, which differs from our Fig. 3. This shows that their quantum phases on both sides of the critical values (which are numerically different for these two models) are not the same as ours. Besides, the spin and thermal transport properties are not discussed in their paper.[18]

This work is supported by the NSC of Taiwan under Grant Nos. 91-2112-M-003-019 and 92-2112-M-003-009, and by the National Natural Science Foundation of the People's Republic of China under Grant No. 19974001 and the Education Commission of Anhui.

*Permanent address: Department of Physics, Anhui University, Hefei 230039, Anhui, People's Republic of China.

[1] S. Sachdev, *Quantum Phase Transitions* (Cambridge University Press, Cambridge, 1999).
[2] H. Yoshizawa, G. Shirane, H. Shiba, and K. Hirakawa, Phys. Rev. B **28**, 3904 (1983).
[3] E. Lieb, T. Schultz, and D. Mattis, Ann. Phys. (N.Y.) **16**, 407 (1961).
[4] A. M. Tsvelik, Phys. Rev. B **42**, 779 (1990).
[5] H. Frahm, J. Phys. A **25**, 1417 (1992).
[6] See Z. Racz, J. Stat. Phys. **101**, 273 (2000), and the references therein.
[7] M. Muramoto and M. Takahashi, J. Phys. Soc. Jpn. **68**, 2098 (1999); also, see A. A. Zvyagin and A. Klumper, Phys. Rev. B **68**, 144426 (2003).
[8] This generalized stiffness is analogous to the charge stiffness introduced by W. Kohn in 1964 as a criterion of conducting or insulating phase at $T=0$ in the context of the Mott-Hubbard transition [see Phys. Rev. **133**, A171 (1964)].
[9] X. G. Wen, F. Wilczek, and A. Zee, Phys. Rev. B **39**, 11 413 (1989).
[10] H. Frahm and C. Rodenbeck, J. Phys. A **30**, 4467 (1997).
[11] X. Zotos and P. Prelovsek, in the book series, Physics and Chemistry of Materials with Low-Dimensional Structures, Interacting electrons in low dimensions (to be published) or see cond-mat/0304630.
[12] F. Heidrich-Meisner, A. Honecker, D. C. Cabra, and W. Brenig, Phys. Rev. B **66**, 140406(R) (2002).
[13] E. Orignac, R. Chitra, and R. Citro, Phys. Rev. B **67**, 134426 (2003).
[14] X. Zotos, Phys. Rev. Lett. **82**, 1764 (1999).
[15] The same quantity for $\alpha=0$ but $\Delta\neq 0$ has been calculated by A. Klümper and K. Sakai, J. Phys. A **35**, 2173 (2002).
[16] K. Okunishi, Y. Hieida, and Y. Akutsu, Phys. Rev. B **60**, R6953 (1999).
[17] T. Yamamoto, R. Manago, Y. Mori, and C. Ishii, J. Phys. Soc. Jpn. **72**, 3204 (2003).
[18] I. Titvinidze and G. I. Japaridze, Eur. Phys. J. B **32**, 383 (2003).